University of Texas Rio Grande Valley

ScholarWorks @ UTRGV

2020

Nature inspired solid–liquid phase amphibious adhesive

Alin Cristian Chipara

Gustavo Brunetto

Sehmus Ozden

Henrik Haspel

Partha Kumbhakar

See next page for additional authors

Authors

Alin Cristian Chipara, Gustavo Brunetto, Sehmus Ozden, Henrik Haspel, Partha Kumbhakar, Ákos Kukovecz, Zoltán Kónya, Robert Vajtai, Mircea Chipara, and Douglas S. Galvao

Nature inspired solid-liquid phase amphibious adhesive

Journal:	Soft Matter
Manuscript ID	SM-ART-01-2020-000105.R1
Article Type:	Paper
Date Submitted by the Author:	17-Mar-2020
Complete List of Authors:	Chipara, Alin; Rice University, Materials Science Brunetto, Gustavo; Universidade Estadual de Campinas Özden, Şehmus; Los Alamos National Laboratory, Materials Physics and Applications Division Haspel, Henrik; King Abdullah University of Science and Technology Kumbhakar, Partha; National Institute of Technology, Physics Kukovecz, Akos; Univ Szeged, Applied & Environmental Chamistry Konya, Zoltan; University of Szeged, Applied & Environmental Chamistry Vajtai, Robert; Rice University, Chipara, Mircea; UTRGV, Department of Physics and Astronomy Galvao, D.; State University of Campinas, Applied Physics Tiwary, Chandra; Rice University, Materials Science and NanoEngineering Ajayan, Pulickel; Rice University, Mechanical Engineering and Materials Science

Nature inspired solid-liquid phase amphibious adhesive

Alin Cristian Chipara,[1] Gustavo Brunetto,[1,2] Sehmus Ozden,[1] Henrik Haspel,[1,3] Partha Kumbhakar,[7] Ákos Kukovecz,[3,5] Zoltán Kónya,[3,6] Robert Vajtai,[1] Mircea Chipara,[4] Douglas S. Galvao,[2] Chandra Shaker Tiwary,[1,7*] and Pulickel M. Ajayan[1*]

Here we report a new class of bio-inspired solid-liquid adhesive, obtained by simple mechanical dispersion of PVDF (polyvinylidene fluoride) (solid spheres) into PDMS (polydimethylsiloxane) (liquid). The adhesive behavior arises from strong solid-liquid interactions. This is a chemical reaction free adhesive (no curing time) that can be repeatedly used and capable of instantaneously joining a large number of diverse materials (metals, ceramic, and polymer) in air and underwater. The current work is a significant advance in the development of amphibious multifunctional adhesives and presents potential applications in a range of sealing applications, including medical ones.

Frequently, nature is used as a source of inspiration for researchers in the development of new functional materials.[1,2] Among all bio-mimetic materials, particular interest has been paid to soft temporary adhesive materials due to their potential applications in consumer products: biomedical, robotics, and device packaging.[3–5] Materials based on geckos and spiders [6,7] are some of the earliest examples of adhesive materials which have been further improved through the addition of nanomaterials and enhanced processing.[8,9] In all of them, the core mechanism is based on intermolecular forces that arise from van der Waals and hydrogen bonding interactions.[10,11] Generally, the dispersive force exceeds the other types of interactions in ambient conditions but does not have significant resistance whilst submerged in water.[11,12] Great effort has been expended on the synthesis of adhesive materials inspired by mussels, due to their ability to work underwater.[13] In general, these materials rely on chemical bond formations with the substrate, which are unaffected by water.[13] However, one of the drawbacks of this approach is the large variation in bond strength with different substrates. As an alternative, researchers have yet again found inspiration in nature, specifically in the adhesion behavior of the tree frog, leading to the development of novel environmentally independent (in air or underwater) sticky materials.[14]

The main mechanism of tree-frog adhesion is a combination of complex geometry coupled with the discharge of a viscous fluid. Generally, the geometry is composed of a hexagonal array of nano-pillars distributed randomly within the array and filled with a viscous fluid.[15] Several experimental and theoretical studies suggested contributions from capillary forces, friction, and viscous forces to the wet adhesion mechanism.[16] The draining effect associated with the channel structures allows the frogs to expel the fluid out of the contact layer and achieve high frictional forces. There have been recent reports suggesting the role played by a second phase fluid added to sticky matrices.[17,18] Cheung et. al.[19] demonstrated a simple method to enhance adhesion by depositing a thin layer of silicon oil into an array of bio-mimetic fibers. Meanwhile, Patilet. et. al.[20] coated a layer of liquid PDMS with low cross-linker content on an array of micro-posts and found enhanced adhesion with limited magnitude of deformation as well as less cohesive separation. All these approaches, however, involve complex fabrication processes and stabilizing solid-liquid interfaces.

In our previous work[21], we focused on the adhesive property of polytetrafluoroethylene (PTFE) and PDMS. In this study, we have investigated the adhesive nature of PVDF and PDMS composites. PVDF is a common and easily available polymer. PTFE has three fluorine atoms per monomer whereas PVDF has just one. We also demonstrated that the strength of the adhesive can be tuned just engineering the number of fluorine atoms in the monomers. Also, this new developed

[1]Department of Materials Science and Nano Engineering, Rice University, Houston, TX, 77005, USA

[2]Department of Applied Physics and Center for Computational Engineering and Sciences, State University of Campinas, Campinas, SP, 13083-959, Brazil

[3]Department of Applied and Environmental Chemistry, University of Szeged, RerrichBélatér 1, Szeged H-6720, Hungary

[4]Department of Physics and Geology, University of Texas-Pan American, Edinburg, TX 78539, USA

[5]MTA-SZTE "Lendület" Porous Nanocomposites Research Group, RerrichBélatér 1, Szeged H-6720, Hungary

[6]MTA-SZTE Reaction Kinetics and Surface Chemistry Research Group, RerrichBélatér 1, Szeged H-6720, Hungary

[7]Metallurgical and Materials Engineering, Indian Institute of Technology Kharagpur, Kharagpur-721302, India.

Corresponding Authors: E-mail: ajayan@rice.edu (P. M. Ajayan), cst.iisc@gmail.com (C. S. Tiwary)

simple amphibious adhesive can act as more universal glue that performs well with a number of materials in a wide rande of conditions. We report a chemical reaction free, scalable approach to create a two-phase (solid/liquid) polymer adhesive material (repeatedly stick to different materials, independent of environment, does not require curing time) achieved by combining two inexpensive commercial polymers (PDMS and PVDF). At the macroscopic level isolated PDMS is a transparent liquid, whereas PVDF is a white powder. We chose to use PVDF in the form of solid spheres due to its large surface area and a liquid form of PDMS due to the large elasticity of the polymer chain allowing it to readily interact with the F atoms. The solid-liquid composite results from the simple mechanical dispersion of the PVDF into PDMS, as

shown in Fig. 1A. Just combining these two polymers the resulting material is no longer solid or liquid but has a gel-like consistency and a translucent color (shown in Fig. 1B, see the coating of adhesive on the glass covering right owl eye) and Fig. 1D-E illustrates the gel consistency. The structural characterization at the microscopic level and subsequent proof of the PVDF dispersion into PDMS was obtained by optical and scanning electron microscopy (SEM) (Fig. 1C-F). The images show a well-dispersed blister-like appearance of solid PVDF spheres (~200 nm diameter) embedded into liquid PDMS. The material also shows structural and chemical stability over long periods of time (no segregation or degradation were observed in samples aged up to several months).
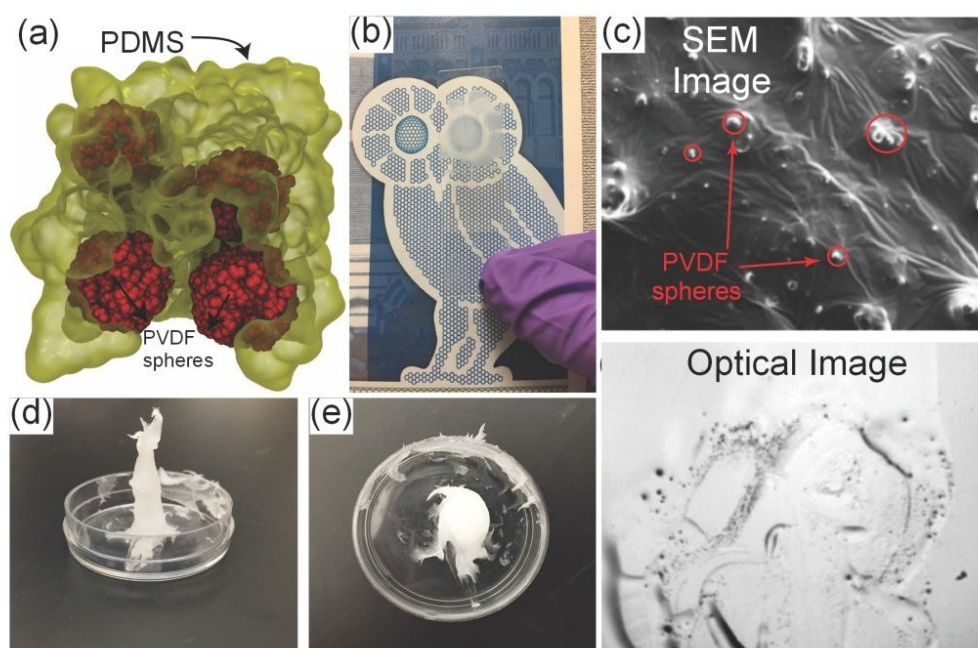

Fig. 1: Structural characterization of the material resulting from combining (mechanical dispersion) of PVDF and PDMS. (A) The molecular model composed of PVDF rigid spheres (in red) embedded into the liquid PDMS phase (in yellow). (B) Digital image of a glass sheet coated with the adhesive showing the translucent material. (C) SEM image showing the PVDF spheres immersed into the PDMS medium. (D) Side view and (E) top view of the processed adhesive. (F) Optical image of the adhesive depicting the uniform dispersion of solid PVDF (black) into liquid PDMS (white).

Diversified spectroscopy analyses (Raman, Fourier Transform Infrared (FT-IR) and X-Ray Diffraction (XRD)) reveal that the signatures belonging to isolated PVDF and PDMS are preserved after mechanical dispersion (Fig. S1 to S8 - supplementary material). The Thermogravimetric Analysis (TGA) of the adhesive shows degradation occurred at $(461\pm1)^{o}C$ and a small broad peak can be observed at $(439\pm1)^{o}C$ (Fig. S1C –supplementary material). The onset of degradation was shifted in relation to neat PVDF, which can be attributed to the interactions between the two polymers. The adhesive composite shows an enhancement of thermal stability compared to pure PVDF due to the addition of PDMS and it is a consequence of the strong interactions between PVDF and PDMS.

These results indicate that no chemical reaction between the polymers occurred during the process (two-phase system remains and no new phase forms). In order to gain insight into the PDMS/PVDF interface, we carried out Density Functional Theory (DFT) calculations. DFT was used to analyze how the relative orientation between PDMS and PVDF chains affect adhesive stability. The DFT study was carried out considering PDMS and PVDF short chains (Fig. 2 A-B).

The interaction energy is calculated for different configurations (Fig. S9 - supplementary material). The interaction energy is defined as the difference between the total energy of the interacting chains and the total energy for the isolated ones, i.e., $E_{TOT} = E_{PVDF+PDMS} - (E_{PDMS} + E_{PVDF})$ (see supplementary material for details about the simulations). In Fig. 2C-E we show the three most stable configurations, in

terms of interaction energies (Fig. 2F). These large differences can be explained by the electronic cloud chain anisotropy. The results show that the interaction energy is strongly dependent on the relative orientation between the chains, which resembles the lock and key effect present in similar molecular systems.[22]

The electronic density for configuration 3 (Fig. 2C) shows a substantial overlap between the chains when compared with other considered configurations (e.g. configurations 5 and 6, Fig. 2D-E). Electronic density overlap is evidence of strong interactions (e.g. hydrogen bonding)[23] between PDMS and PVDF, especially in configuration 3. For the other configurations, the overlap is less pronounced and indicates a weaker interaction such as adsorption.[24] Energetic comparison for all the considered configurations showed a preferential orientation and the strength of the interaction (~1.0 eV) comparable to the ones encountered in the ionic HF system.[25,26] These results have important implications to explain the adhesive properties, as discussed below.
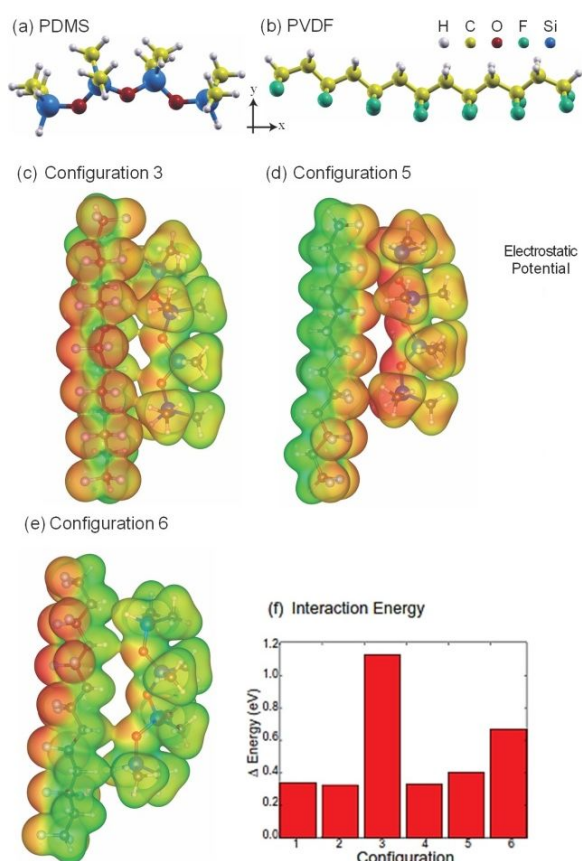

Fig. 2: **Dipole interaction between PVDF and PDMS polymers.** (A) PDMS and (B) PVDF chains considered in the DFT calculations. Taking the chain length as reference (x-direction) the upper region is formed mostly by hydrogen, while the bottom one is formed by oxygen (fluorine) for PDMS (PVDF) (C), (D) and (E) show the electronic density for the three most stable configurations. (F) Interaction energy (in eV) for all the considered configurations. To allow a direct comparison between the electronic densities, all of them were plotted with the same iso-surface value.

In order to characterize the adhesive properties, cyclic compressive measurements (loading-unloading) with 0.01, 0.05 and 0.10 N were performed (Fig. 3A). During adhesive loading (compression) the stiffness increases and during unloading (release) the stiffness does not drop, which is a signature of adhesion. As it can be seen from our results, as we increase the load the stiffness also increases, which can be due to the flow of liquid PDMS in between solid PVDF spheres. As the distance between them is decreased it results in higher stiffness due to surface interaction of PVDF and PDMS. Similar behavior is also reflected in strain (Fig. S10, supplementary information). The adhesion behavior can be repeated for more than 20 cycles and we do not observe any change in stiffness (Fig. S10). In order to quantify the strength of the adhesive, a 180-degree peeling test (as schematically shown in the inset of Fig. 3B) was performed using two copper sheets. The shear stress versus strain plot (Fig. 3B) shows a linear stress region until 2% strain and reaches a maximum value (ultimate strength) around 1.1 MPa (Fig. 3B - point A). Increasing the strain further from 2 to 10% we observed that the stress decreases (the region between points A and D, Fig. 3B. The conventional single use adhesive joint reaches maximum and fails rapidly. In current adhesive the does not allows it to fail rapidly, rather fails gradually which are marked here as different points (B, C, D). The current adhesive works on atom interaction of solid-liquid interaction. During failure the solid particle embedded in liquid slides on the liquid, due to surface interaction it provides resistance. In order to understand the morphology changes during adhesion, two glass sheets were joining together (containing adhesive in between - before the stage in Fig. 3C). The glass sheets are then separated and the process is monitored using an optical microscope. As the sheets are pulled, the adhesive exhibits severe plastic extensions and formation of strings (Fig. 3C - after). This behavior is observed in most adhesives.[27] The SEM image of the separated sheets (Fig. 3D), also confirms the presence of strings. A higher magnification image (Fig. 3E) shows the presence of strain lines running across their surfaces of the strings. These strain lines indicate adhesive stress accommodation, which is a consequence of PVDF spheres acting as anchor points in PDMS. The same behavior cannot be seen in isolated PDMS (Fig. S13 - supplementary material). Further evidence of anchoring effect was obtained through Atomic Force Microscopy (AFM). AFM height profile (Fig. 3F) revealed a peak of 200 nm (corresponds to PVDF size) followed by steps around it. The steps correspond to strain lines in the PDMS due to surface interactions between the PVDF and PDMS which anchor the PVDF in place.

DFT results showed that there are significant interaction energy differences, which could be in the origin of the anchoring effect. To address this issue with DFT methods is computer prohibitive (size system and simulation time). One possibility is to use classical Molecular Dynamics (MD) for large enough systems to mimic the PDMS/PVDF structures.
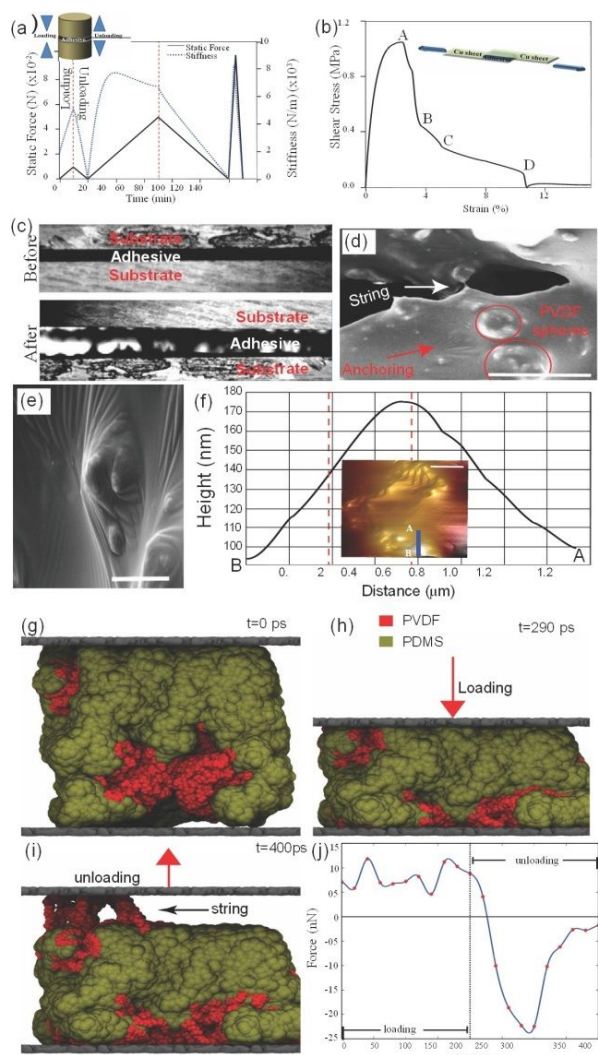
Fig. 3: Mechanical testing of the adhesive. (A) Cyclic test of compression (loading) and tensile (unloading). The loading/unloading stages are indicated by dotted red lines. The black solid and dotted blue curves indicate the load and stiffness variation in time, respectively. Inset shows schematic of the loading setup. (B) Adhesive shear test (180-degree peel test) of two copper samples put into contact using the adhesive. Inset shows schematic of the loading conditions (C) Optical imaging shows two glass sheets stick together by the adhesive (before) and the formation of strings during separation (after). (D) SEM image after separation highlighting a single string. (E-G) Snapshots from MD simulations mimicking the loading/unloading adhesive cycle (E) initial stage, (F) maximum loading and (G) intermediate unloading stage showing the string formation. (H) The force profile experienced by the adhesive during the load (positive force) and unload (negative force). The red points indicate the force

at a specific time of the simulation and the blue curve is the fitting of these points. (I) High magnification SEM image, (J) and AFM image with line profile of strings after adhesive detachment.

Using this approach, it is possible to address the adhesive behavior from atomistic level. We have carried out MD simulation using classical force field[28–31] (see methodology section for further information). The used model system (Fig. 3G) consists of PVDF spheres (in red) embedded into the PDMS medium (in yellow) placed in between two slabs of amorphous silicon oxide (SiO_2). To simulate the load stage, the distance between the slabs is decreased by a constant rate until to attain a significant deformation (54%) (Fig. 3H). During the adhesive compression, the liquid phase allows the solid spheres to easily flow towards the slabs, thus increasing the contact area. The unload stage is performed using the same loading rate but along the opposite direction (Fig. 3I). In this stage, it is possible to observe the onset of string formation between the slabs, which are very similar to experimental observations (Fig. 3D). The net force along the direction of the sheet displacement is recorded during the load/unload cycle. We can identify an asymmetric behavior (Fig. 3J), with maximum force for the loading stage (corresponding the instant from 0 to 200 ps) ~12 nN and for the unloading stage (corresponding the instant from 200 to 400 ps) ~25 nN. The force experienced during the unloading stage is around two times higher than the maximum force in the loading stage, which characterize an adhesive regime.

The combined analysis of experiments and simulations allow us to have a clear understanding of the adhesive mechanism. Although individually PDMS and PVDF do not show adhesive behavior due to the absence of strong dipolar interactions, after mechanical dispersion, the composite does. During the loading, PVDF interacts stronger than PDMS with the contact surface, while during the unloading due to the strong interaction between the PDMS and PVDF we have an anchor effect that is the origin of the adhesive behavior and string formation.

Our adhesive can work on a broad range of different materials (and also a combination of them), such as organic, inorganic, metal and oxide (Fig. 4A-D). For all cases, standard weights were used to determine the maximum shear strength required for separation. We have explored the application of the adhesive in sticking bio-materials, such as chicken and pig skins (Fig. 4C-D). The measured adhesive shear stresses of a few of these materials are also shown in Fig. 4E. This universal-like adhesion can be explained by the coexistence of liquid and solid dynamics. While the liquid can take the shape (roughness of the surface) of the interface creating an almost perfect interface and the size of the nanoparticles allows an almost homogeneous distribution, creating a strong interface interaction (Fig. S14).

To evaluate the adhesion behavior of the composite in liquid media (water and oil), a cycling loading and unloading test in

ARTICLE

submerged conditions is performed (Fig. 4G). The submerged clamp volume is filled with different fractions of water and compressed and then pulled. The adhesive behavior is similar in both wet and dry conditions (water and oil, as well).
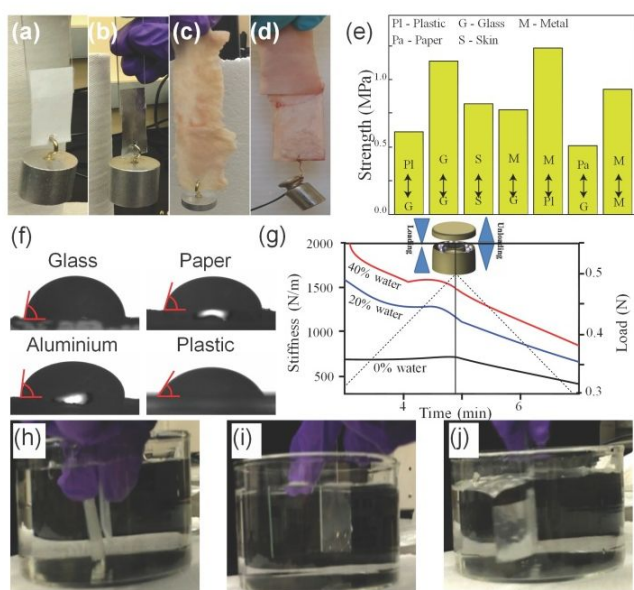

Fig. 4: **Adhesion on different materials and in different environments**. Representative examples of adhesion on different substrates (A) glass/paper, (B) metal/glass, (C) chicken skin and (D) pig skin. (E) Adhesive shear strength for different materials interfaces. (F) Contact angle values of water droplet on glass, paper, aluminum and plastic coated with adhesive. (G) Stiffness versus time under loading and unloading cycle of adhesive submerged with a different fraction of water in a submerged clamp (shown in the inset). (H) Demonstration of adhesion behavior of two transparent glass sheets inside the water initial state of two separated glass sheets. (I-J) adhered glass sheets viewed from different directions.

During the loading of PVDF in PDMS, a strong interaction is formed in between the liquid PDMS and solid PVDF, as confirmed by molecular dynamics simulations and FTIR results. The fluorine atoms of PVDF strongly interacted with PDMS via dipole-dipole or dipole-dipole induced interactions. Generally, polymers have electrostatic attractions due to the presence of large electronegativity differences between the F/H (or other elements) in them. Therefore, adhesives made from those polymers can strongly bond with the other surfaces. In the case of wet surfaces, the side chains of composites adhesive surface of PVDF and PDMS can easily form an intermolecular hydrogen bonding with adjacent water molecules. Therefore, it sticks easily on the wet surfaces. PDMS and PVDF are both hydrophobic materials. We also tested the adhesive wettability to see if the mechanical dispersion changes this characteristic. We used the contact angle measurements (Fig. 4F) as an estimative that the material is indeed hydrophobic. The obtained contact angle values were: Glass = ~70-85°, Paper = ~70-80°, Aluminum = ~70-85°, Plastic = ~40-50°. The

results showed that the adhesive is still hydrophobic (Fig. 4F). The adhesive can even work underwater, as illustrated in Fig. 4H-I (see also video in supplementary material).

We have considered different fractions of the individual polymers. We believe that the optimal mixing ratio is 1:1 as it maximizes the number of F atoms that can interact with the H atoms. A higher fraction of PVDF resulted in poor wetting of adhesion on the surface, whereas a higher fraction of liquid PDMS resulted in low strength. We observed optimum strength and wetting for a 50:50 mixture.

In summary, we report a bio-inspired, chemical-free (with no curing time required), easily scalable, a new class of adhesive, made by simple mechanical dispersion of PVDF (solid) into PDMS (liquid). The material can be universally used for many times and under different ambient conditions, even under liquids. The reason the adhesive can be used multiple times is that the dipole-dipole interactions weaken as the molecules are pulled further apart. However, the material does not structurally change and the interactions can re-form once the two substrates are pressed again back into contact with each other.

Based on our study, we can conclude that our composite should stick to any material that makes bonding with F-, and wets PDMS. These results represent a significant advance in achieving amphibious adhesive and can lead to new pathways for designing new universal adhesives, similar to the ones exhibited by some of the biological systems in nature.

Conflicts of interest

There are no conflicts to declare.

Acknowledgements

Materials and Methods

One possible way to synthesize a PVDF-PDMS solid-liquid composite material is by using a rigorous mixing-evaporation process. Although the basic constituents of this material are similar to what is reported here, the phase composition, distribution, and morphology of the two material is distinctly different due to the different processing used to disperse the phases in the material. The obtained material using the mixing-evaporation process is a white solid powder (unlike of the gel-like material obtained here) and shows an interesting self-stiffening behavior during loading. We expect that the particle size plays a role in the strength of the adhesive. Smaller particles will have more surface area which can result in more chemical interaction and hence strength. The large

electronegativity of fluorine atoms in PVDF delocalizes the electron distribution of neighbouring atoms by generating dipole and dipole induced moments, which are responsible for complex dipolar interactions. In the present work we used commercially available PVDF with 200 nm size for all the experiments.

In the current work, the PVDF-PDMS mixture was made through mechanical dispersion of 50 wt. % PDMS and 50 wt. % PVDF, done under ambient conditions. The constant addition of PVDF into the system showed an optical shift from the clear nature of PDMS to an opaque white gel. The blend exhibited a markedly different consistency than the PDMS indicating a change in the system. The properties and structure of the blend were analyzed using microscopy (SEM and Optical), spectroscopy (Raman and FTIR), as well as mechanical (load-unload compressive DMA test) and thermal testing (TGA). To characterize the existing bonds and the interactions within the blend, we used Raman and Fourier Transform Infrared (FTIR) spectroscopy. Raman measurements were carried out using a Bruker Senterra confocal microscope operating at 785 nm.

Characterization

Imaging was done using scanning electron microscopy (SEM) (FEI Quanta ESEM FEG) and a goniometer (Rime-Hart). Raman was done using a Bruker Senterra Raman at 785 nm in ambient conditions. Thermal measurements were done using a TA Instruments Q500 TGA. FTIR was done using a Bruker. XPS was done using a PHI Quantera XPS. XRD was done using a Discovery 8 Bruker XRD. For the mechanical tests, we used Dynamic Mechanical Analysis (DMA). For the load-unload procedure in compression, we considered three cycles with a maximum force of 0.01 N, 0.05 N, and 0.1 N, respectively. Using a blend made of PVDF and PDMS, which has a gel-like consistency, we create a thick layer and performed the load-unload testing. This kind of test allows us to understand how adhesion behaves both when adhering and upon separation from a surface.

Simulations details

We carried out Density Functional Theory (DFT) within the Generalized Gradient Approximation (GGA)[32] and Perdew-Burke-Ernzenhof (PBE)[33] for exchange-correlation functional in the calculations of the electronic properties of PDMS and PVDF. The calculations were carried out using the code OpenMX, which employs a formalism based in pseudo-atomic orbitals (PAO)[34] and norm-conserving pseudopotentials.[35,36,37] For the elements carbon, oxygen and silicon we considered two s-orbitals, two p-orbitals and one d-orbital (s2p2d1) as a PAO basis set to expand the electronic wave function. For hydrogen and fluorine ones the considered basis set were s2p1 and s4p4d4f3, respectively. For energy cutoff and energy convergence tolerances, we used 125 and 1.0×10^{-6} Hartree, respectively. We carried out geometry optimization and the final geometry was considered optimized when the maximum force in the system is below 1.0×10^{-4} Ha/Bohr.

The MD calculations were carried out using LAMMPS[38] software. The bonded interactions (bond, angle and dihedral terms) were described by COMPASS[39] force field, and the parameters optimized to describe the PDMS[40] and PDVF[41] structures. The atoms belonging to the SiO_2 slabs were kept frozen during the simulations. To simulate the loading procedure, a mixture of PDVF and PDMS was placed in between two SiO_2 slabs. The bottom slab was kept fixed and the upper one had all atoms displaced by a constant rate of 1.5×10^{-4} Ang/fs, approximating to the bottom one. The unloading procedure was performed using the same rate but in the opposite direction.

References

1   E. Munch, M. E. Launey, D. H. Alsem, E. Saiz, A. P. Tomsia and R. O. Ritchie, *Sci.*, 2008, **322**, 1516–1520.
2   L. J. Bonderer, A. R. Studart and L. J. Gauckler, *Sci.*, 2008, **319**, 1069–1073.
3   Y. Li, K. Moon and C. P. Wong, *Sci.*, 2005, **308**, 1419–1420.
4   J. H. Waite, *Nat Mater*, 2008, **7**, 8–9.
5   T. M. Shazly, A. B. Baker, J. R. Naber, A. Bon, K. J. Van Vliet and E. R. Edelman, *J. Biomed. Mater. Res. -Part A*, 2010, **95**, 1159–1169.
6   P. R. Jones, X. Hao, E. R. Cruz-Chu, K. Rykaczewski, K. Nandy, T. M. Schutzius, K. K. Varanasi, C. M. Megaridis, J. H. Walther, P. Koumoutsakos, H. D. Espinosa and N. A. Patankar, *Sci. Rep.*, 2015, **5**, 12311.
7   S. W. Cranford, A. Tarakanova, N. M. Pugno and M. J. Buehler, *Nature*, 2012, **482**, 72–76.
8   A. Tuteja, W. Choi, M. Ma, J. M. Mabry, S. A. Mazzella, G. C. Rutledge, G. H. McKinley and R. E. Cohen, *Sci.*, 2007, **318**, 1618–1622.
9   S.-M. Lee, E. Pippel, U. Gösele, C. Dresbach, Y. Qin, C. V. Chandran, T. Bräuniger, G. Hause and M. Knez, Sci., 2009, **324**, 488–492.
10   L. Qu, L. Dai, M. Stone, Z. Xia and Z. L. Wang, *Sci.*, 2008, **322**, 238–242.
11   H. Lee, B. P. Lee and P. B. Messersmith, *Nature*, 2007, **448**, 338–341.
12   C. Zhong, T. Gurry, A. A. Cheng, J. Downey, Z. Deng, C. M. Stultz and T. K. Lu, *Nat Nano*, 2014, **9**, 858–866.
13   A. R. Scott, *Nature*, 2015, **519**, S12–S13.
14   J. Iturri, L. Xue, M. Kappl, L. García-Fernández, W. J. P. Barnes, H.-J. Butt and A. del Campo, *Adv. Funct. Mater.*, 2015, **25**, 1499–1505.
15   D.-M. Drotlef, L. Stepien, M. Kappl, W. J. P. Barnes, H. J. Butt and A. D. Campo, *Adv Funct Mater*, 2013, **23**, 1137–1146.
16   T. Endlein, W. J. P. Barnes, D. S. Samuel, N. A. Crawford, A. B. Biaw and U. Grafe, *PLoS One*, 2013 ,**8**, e73810-e73821.
17   D. M. Drotlef, E. Appel, H. Peisker, K. Dening, S. N. Gorb and W. J. P. Barnes, *Interface Focus*, 2015, **5**, 1–11. http://dx.doi.org/10.1098/rsfs.2014.0036
18   G. Hanna and W. J. Barnes, *J. Exp. Biol*, 1991, **125**, 103–125.
19   E. Cheung and M. Sitti, *J. Adhes.*, 2011, **87**, 547–557.
20   S. Patil, R. Mangal, A. Malasi and A. Sharma, *Langmuir*, 2012, **28**, 14784–14791.

Please do Soft Matter margins

21. A. C. Chipara, T. Tsafack, P. S. Owuor, J. Yeon, C. E. Junjermeier, A. C. T. van Duin, S. Bhowmick, S. A. S. Asis, S. Radhakrishnan, J. H. Park, G. Brunetto, B. A. Kaipparettu, D. S. Galvao, M. Chipara, J. Lou, H. H. Tsang, M. Dubey, R. Vatjai, C. S. Tiwary, and P. M. Ajayanm *Mater. Chem. Today,* 2018, **9**, 149-157.

22 R. Otero, F. Hümmelink, F. Sato, S. B. Legoas, P. Thostrup, E. Laegsgaard, I. Stensgaard, D. S. Galvão and F. Besenbacher, *Nat. Mater.*, 2004, **3**, 779–782.

23 T. A. Wesolowski, *J. Am. Chem. Soc.*, 2004, **126**, 11444–11445.

24 J. Zhao, A. Buldum, J. Han and J. P. Lu, *Nanotechnology*, 2002, **3**, 195–200

25 J. W. Larson and T. B. McMahon, *Inorg. Chem*, 1984, **10**, 2029–2033.

26 J. Emsley, *Chem. Soc. Rev.*, 1980, **9**, 91–124.

27 K. Kendall, N. A. Peppas, T. Nagai and P. Tech-, *Adv. Sci.*, 2011, **263**, 1720–1725.

28 K. Vanommeslaeghe, E. Hatcher, C. Acharya, S. Kundu, S. Zhong, J. Shim, E. Darian, O. Guvench, P. Lopes, I. Vorobyov and A. D. Mackerell, *J. Comput. Chem.*, **31**, 671–690.

29 R. A. Buckingham, *Proc. R. Math. Phys. Eng. Sci.*, 1938, **168**, 264–283.

30 C. Sun, *J Phys Chem B*, 1998, **102**, 7338–7364.

31 W. L. Watkins, *J Phys Chem A*, 2001, **105**, 4118–4125.

32   P. Perdew *et al.,*. *Phys. Rev. B*. 1992, **46**, 6671–6687.

33. J. P. Perdew, K. Burke and M. Ernzerhof, *Phys. Rev. Lett.* 1996, **77**, 3865–3868.

34. T. Ozaki, *Phys. Rev. B*. 2003, **67**, 155108.

35. G. B. Bachelet, D. R. Hamann and M. Schlüter, *Phys. Rev. B*. 1982, **26**, 4199–4228.

36. N. Troullier and J. L. Martins, *Phys. Rev. B*. 1991, **43**, 1993–2006.

37. S. Grimme, *J. Comput. Chem.* 2006, **27**, 1787–1799.

38. S. Plimpton, *Journal of Computational Physics*. 1995, **117**, 1–19.

39. H. Sun, *J. Phys. Chem. B*. 1998, **102**, 7338–7364.

40. J. S. Smith, O. Borodin and G. D. Smith, *J. Phys. Chem. B*. 2004, **108**, 20340–20350.

41. N. Karasawa and W. Goddard, *Macromolecules* 1992, **25**, 7268–7281.

Please do not adjust margins